TECHNOLOGY DEVELOPMENT FOR EXOPLANET MISSIONS

Technology Milestone Report
Hybrid Lyot Coronagraph Technology – Linear Masks

John Trauger, P.I.
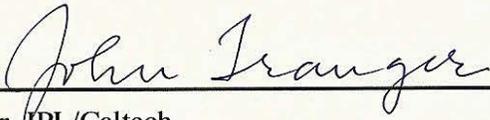*Brian Gordon, John Krist, Dimitri Mawet,*
Dwight Moody, and Peggy Park

15 December 2012

APPROVALS

Released by

John Trauger 2/26/2013
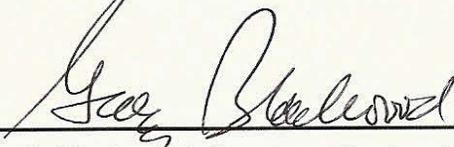
John Trauger, JPL/Caltech

Approved by

2/26/2013
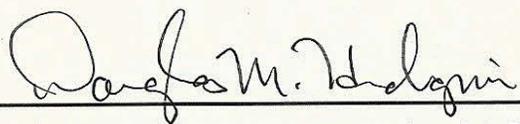
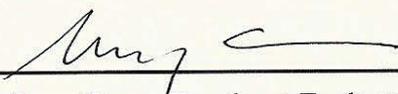Peter R. Lawson, Exoplanet Exploration Program Chief Technologist, JPL

2/28/2013

Marie Levine, Exoplanet Exploration Program Technology Manager, JPL

3/3/2013

Gary H. Blackwood, Exoplanet Exploration Program Manager, JPL

3/5/2013

Douglas Hudgins, Exoplanet Exploration Program Scientist, NASA HQ

3/5/2013

Anthony Carro, Exoplanet Exploration Program Executive, NASA HQ

Table of Contents

TDEM Milestone Report:
Advanced Hybrid Lyot Coronagraph Technology

1. Overview of this report

We report the results of our ROSES Technology Development for Exoplanet Missions (TDEM) research in pursuit of *Advanced Hybrid Lyot Coronagraph Technology*. We make reference to our June 2010 White Paper that specified the milestone objectives, success criteria, and methodology for computing the milestone metrics. This report follows the general outline of that White Paper, but now describes the mask fabrication and calibration, testbed preparations, the HCIT technology demonstrations, analysis of the results, further steps taken for improved performance, and prospects for future research. We begin with a summary of TDEM accomplishments covered in this report.

Main accomplishments

1. We have designed (with a new integrated occulter/wavefront optimization method) and manufactured (with a deposition system and calibration methods developed in our laboratory) linear hybrid Lyot coronagraph masks with enabling performance for an exo-Earth coronagraphic imaging mission. These design and manufacturing methods have been described in Trauger et al. (2011).

2. We have demonstrated the contrast performance of the hybrid Lyot coronagraph on the HCIT, with raw contrasts at 3 λ_o/D inner working angles (IWA) that exceed all published results we are aware of in bandwidths $\delta\lambda/\lambda_o$ of 2%, 6%, 10%, and 20%.

3. However, we *did not meet* our formal contrast objective at 20% bandwidth (BW). We identified, through model analysis and inspection of fabrication hardware, a calibration error that explains our limiting experimental contrast. We remedied the calibration problem and have manufactured a new corrected mask, ready for a future round of HCIT contrast demonstrations at 20% BW.

4. We carried out the first demonstrations of broadband wavefront sensing and control for high contrast in 6.5% BW filters, a significant advance towards efficient broadband nulling that will be required for space mission operations.

5. Finally, we have designed a new class of circular hybrid masks, now with 2.5 λ_o/D IWA and BWs of 18%, 24%, and 27%, to be further developed, fabricated, and demonstrated in a future effort.

Secondary accomplishments

1. We have developed a software package that integrates mask design, wavefront sensing and control, dark field nulling procedures, and real-time testbed control – and exercised the package for the hybrid Lyot coronagraph design, for automated control of our HCIT experiments, and for high-fidelity modeling of the testbed for experiment diagnostics and performance analysis.

2. We installed a new 64×64 mm DM on the HCIT, including a repolish and recoating of the DM at Xinetics for $\lambda/60$ rms surface figure in the vacuum, fabricated mounting

hardware for the DM and its 4096-channel electronic driver system, purchased a dedicated computer and wrote the control software for the DM driver system.

3. We assembled and aligned the first new layout of the HCIT table in over eight years, incorporating new 1500 mm focal length OAPs to include more DM actuators within the active pupil and longer f/numbers at the coronagraph focal plane. This new Lyot table layout and DM system has since been used by five HCIT investigators (Serabyn, Murakami, Trauger, Shaklan, and Noecker).

4. We have integrated a grism into the HCIT optical system, enabling in-situ measurement of the end-to-end source spectrum, as required for broadband performance certification.

We now return to the milestone narrative, largely verbatim from the June 2010 White Paper.

2. Description of the technology milestone

TDEM Technology Milestones are intended to document progress in the development of key technologies for a space-based mission that would detect and characterize exoplanets, such as ACCESS (Trauger et al. 2008, 2009, 2010), thereby to help gauge the mission concept's readiness to proceed from pre-Phase A to Phase A.

This milestone addresses broadband starlight suppression. ACCESS was designed for high-contrast coronagraphic imaging in three discrete photometric bands spanning an overall 483–880 nm spectral range. The objective of this TDEM milestone is the validation of a new hybrid Lyot focal plane mask in a single 20% spectral band within that nominal range.

The approach for this milestone builds upon that for TPF-C Milestones #1 and #2, which respectively demonstrated monochromatic and broadband (10%) starlight suppression in the High Contrast Imaging Testbed (HCIT). This milestone focuses on the validation of one key TDEM technology – the hybrid Lyot mask. It is more ambitious than the TPF-C Milestones in that a smaller inner working angle and broader spectral bandwidth are attempted. Success is defined in terms of statistically significant performance demonstrations of this key technology, ideally with minimal sensitivity or dependence on extraneous testbed environment factors.

This milestone reads as follows:

Milestone definition:
Starlight Suppression with Linear Hybrid Lyot Masks

Use a linear hybrid Lyot mask to demonstrate coronagraph contrast of 1×10^{-9} at angular separations of $3\lambda_o/D$ and greater in a single 720–880 nm $(\delta\lambda/\lambda_o = 20\%)$ spectral band.

The width of the "spectral band" is defined as the ratio $\delta\lambda/\lambda_o$ where, $\delta\lambda$ is the full width at half maximum (FWHM) transmittance of the band-defining optical filter and λ_o is the central wavelength. The "angular separation" and "inner and outer working angles" are defined in terms of the central wavelength λ_o and the diameter D of the aperture stop on the deformable mirror (DM), which is the pupil-defining element of the laboratory

coronagraph. For this milestone, a hybrid mask has been fabricated with physical dimensions for a $3\lambda_o/D$ inner working angle in an f/31.25 beam, corresponding to the newly reconfigured HCIT with a 48-mm diameter pupil stop at the deformable mirror.

This milestone demonstration includes three specific criteria called out in the TDEM solicitation, as follows.

(1) Demonstration of milestone performance must be stable and repeatable, thereby demonstrating that the result is not spurious or transient. While the coronagraph mask technology is inherently stable, the milestone demonstrations are repeated in order to build up statistical significance at the 90% confidence level, as further described in Section 3.1.7.

(2) Modeling of the milestone must be consistent with the demonstrated result, thereby establishing that the behavior is thoroughly understood. Optical models for testbed coronagraph performance have been developed by our team. Our optical propagation models, based on the Fresnel approximation, incorporate the physical characteristics of the Lyot coronagraph elements, mirror surfaces, the deformable mirror, and the CCD imager. Since the underlying physics is not in question, the accuracy of our model predictions is essentially a test of the fidelity of our physical descriptions of the coronagraph elements. These models consistently predict laboratory contrast performance within ~15%, based on prior demonstrations on the HCIT, including TPF-C Milestones #1 and #2, and on more recent coronagraph demonstrations at 20% bandwidth in support of the ACCESS study.

(3) Error budget for the milestone must be consistent with the models. We rely on our optical models to predict the sensitivity of contrast performance to component imperfections, alignment errors, and sources of drift. The dominant terms in the error budget include the optical characteristics and location of the occulting mask, location of the Lyot stop, stability of the DM surface, and surface quality of the relay optics. For each term in the error budget, we compute the effects of the static error on the achievable contrast (using a standardized speckle nulling computation) and the sensitivity of the achieved contrast to drifts in that term absent further compensation by speckle nulling. A tolerance matrix that includes the error terms known to be most significant at the milestone contrast level (about 10 terms) will be compiled for this milestone report.

2.1. Relevance for a Future Exoplanet Mission

Development of the hybrid Lyot technology is intended to advance the readiness of a mission concept for the coronagraphic imaging and spectroscopic observation of exoplanetary systems. ACCESS serves as a representative probe-class mission concept. A more detailed description can be found in the 176-page ACCESS final report to NASA (Trauger et al. 2009).

To detect exoplanets in the super-Earth to Jovian range, a coronagraph must provide raw image contrast of 10^{-9} in a dark field near the parent star. It is expected that post-processing of coronagraph data will provide detection sensitivities to planets and debris disks an order of magnitude fainter (Trauger and Traub 2007). Therefore, this milestone requires a demonstration of a high contrast dark field at the 10^{-9} level.

4

ACCESS forms a high contrast "dark field" over a working angle spanning 3–22 λ_o/D. The inner working angle (3 λ_o/D) is defined by science requirements, while the outer working angle (~22 λ_o/D) is defined by the highest spatial frequency controlled by a deformable mirror (DM) with 48 actuators across the pupil diameter D. Optical modeling and tolerancing has shown that it is increasingly difficult to control the contrast at field positions closer to the image of the target star. This milestone addresses the most challenging location in the image plane, the inner working angle at the same angular separation as will be required by ACCESS. The contrast specification relates to the average contrast level in the dark field of interest around the source or parent star. This criterion was used in TPF-C milestones #1 and #2, and it is applicable to any coronagraph that propagates its image from sky to the coronagraph focal plane without optical distortions. Analysis of contrast in the dark field must necessarily account for the statistical nature of the speckle patterns, and for the systematic evolution of the speckle patterns by wavelength over the 20% spectral band. The milestone measurements themselves will result in a distribution of speckle intensities, from which we estimate the average contrast and statistical confidence levels, as specified in Section 5 below.

2.2. Hybrid Lyot Coronagraph Masks

Among the four major coronagraph types studied by ACCESS, the hybrid Lyot coronagraph represents the highest readiness level, having demonstrated the best laboratory contrast and bandwidth to date, thereby providing the most reliable estimate of science performance available with today's technology, as well as providing a solid basis for determination of mission cost, risk, and schedule.

Mask design

For a mask design with a single thickness-profiled metallic layer, the initial approach had been to create an attenuation profile with a prescribed band-limited form (Kuchner and Traub 2002), while accepting the resulting phase shifts that necessarily accompany the attenuation in real materials. In general, such "parasitic" phase shifts violate the criteria for band-limited coronagraph masks, and further, these materials may exhibit significant dispersion in optical properties over spectral bandwidths ($\delta\lambda/\lambda_o = 20\%$ or more) that are of interest for exoplanet astronomy (Moody and Trauger 2007, Balasubramanian 2008). The hybrid approach provides a measure of control over phase by adding a thickness-profiled non-absorbing dielectric layer (Moody et al. 2008, Trauger et al. 2011). These masks are composed of metal and dielectric layers superimposed as thickness profiled multilayer coatings on a glass substrate.

The mask design process enables an optimal solution to the non-linear problem of speckle suppression over a range of wavelengths, where the thickness profiles of the metal and dielectric layers, and wavefront phase adjustments with a single deformable mirror are all treated as free parameters. Our multilayer thin film interference code (which generates thickness profiles to match specified attenuation and phase profiles) has been integrated with our wavefront control optimization code (which finds the optimal settings for the deformable mirror in the context of a realistic coronagraph). All computations are carried out within the Fresnel approximation. Our seamless code, written entirely in Python, has been cross checked for the case of our hybrid Lyot designs with John Krist's publicly-available PROPER code, with agreement to within computer rounding errors. Starting with band-limited criteria for the real and imaginary parts of the

occulter attenuation profile at the 800 nm central wavelength, the code generates physically realizable modifications for an optimal balance between spectral bandwidth, contrast, inner working angle, and overall throughput (Figure 1). The predicted contrast performance is shown in Figure 2. This design is described in greater detail in Trauger et al. (2011).
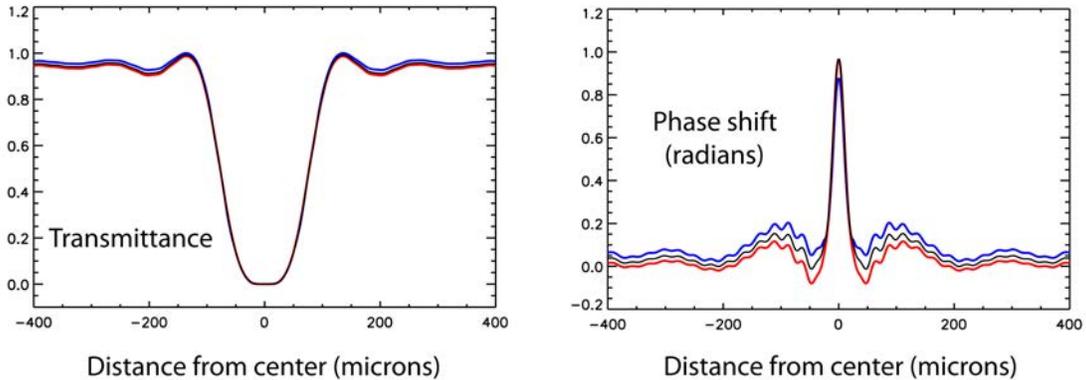

Figure 1. Attenuation and phase shift profiles for the hybrid occulter mask. At left, the attenuation profile reaches 50% transmittance at 3λo/D from center at the central wavelength λo = 800 nm. At right, the transmitted phase profile. Transmittance and phase profiles are shown at three wavelengths: 720 nm (blue curve), 800 nm (black), and 880 nm (red curve). Physical dimensions are scaled to an f/31.25 beam, for which fλo/D = 25 microns at 800 nm.
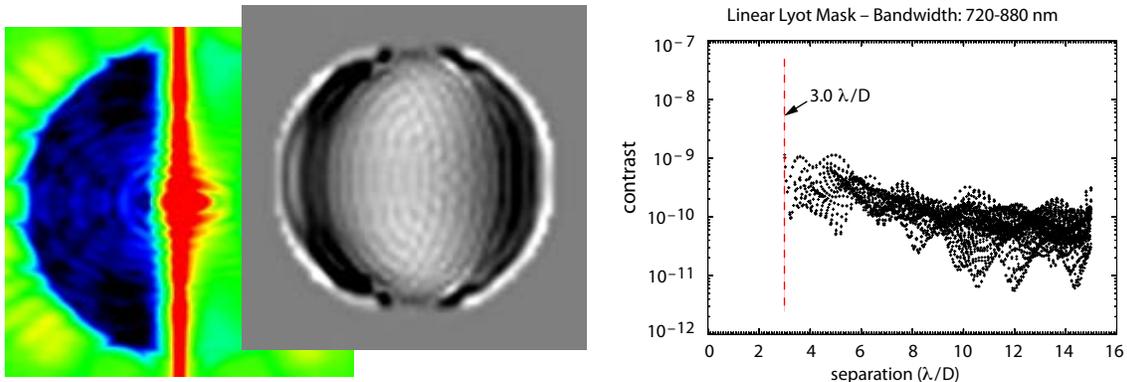
Figure 2. Predicted performance of the hybrid linear Lyot coronagraph, computed with the design software for the mask, a software package that is also used for real-time wavefront sensing and control in the coronagraph experiment. At left, the simulated half-dark field, extending from 3 λo/D to a radius of 15 λo/D. Center, the corresponding phase setting of the deformable mirror. At right, the pixel-by-pixel contrast over the targeted dark field. Predicted contrast is 2×10^{-10} in both the inner dark field (3-4 λo/D) and averaged over the outer (3-15 λo/D) dark field areas.

6

Mask fabrication

On the fabrication side, we have developed the deposition hardware and procedures for improved fidelity of the manufactured metal and dielectric profiles. The optical density and phase shift profiles of the fabricated masks are characterized in detail in our laboratory. Figure 3 is a set of photos of the mask fabrication and test equipment.
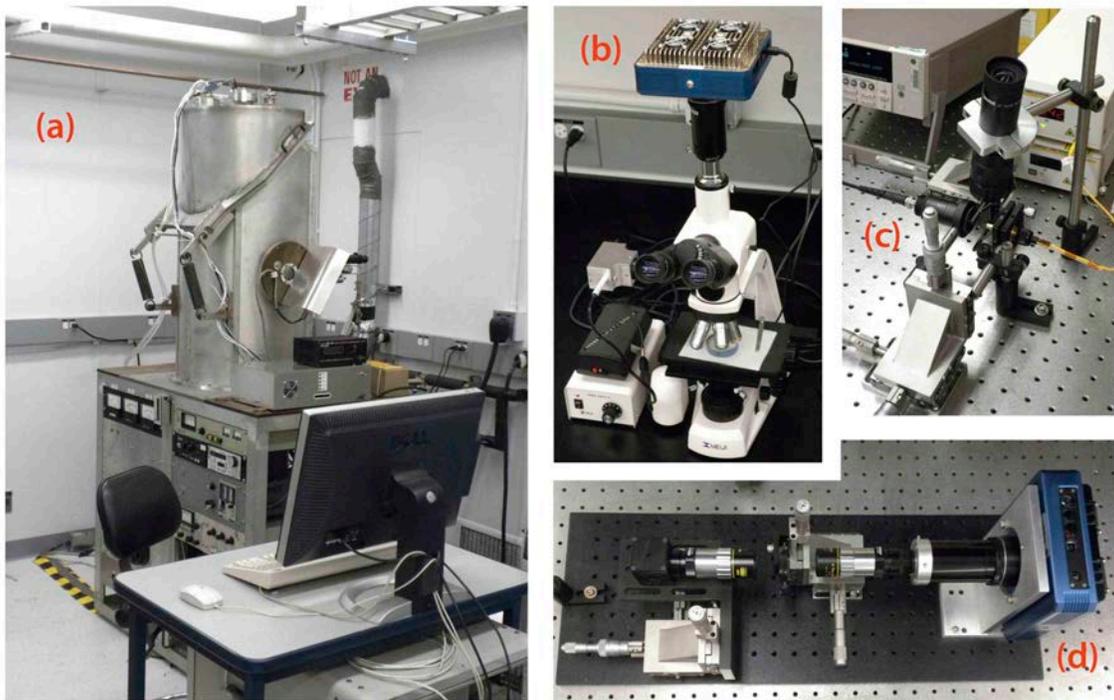
Figure 3. *Laboratory equipment used for the fabrication and characterization of the hybrid Lyot masks. (a) Vacuum thin film deposition system incorporates an e-beam source for metal deposition, a thermal evaporation source for the dielectric, and a computer controlled mechanism for movement of the slit deposition mask. (b) The thickness profile of the dielectric layer is calibrated under the microscope in terms of phase shifts in the dielectric layer measured via Fresnel fringes in 546.1 nm Hg light. (c) The thickness profile of the metal layer is calibrated with a scanning fiber photometer for high contrast measurement of optical density on a 5-micron sample scale. And (d) shows a CCD microscope designed for high contrast imaging of the mask transmittance profile. All equipment resides in the principal investigator's laboratory (JPL 183-818), and is available for further development and mask fabrications.*
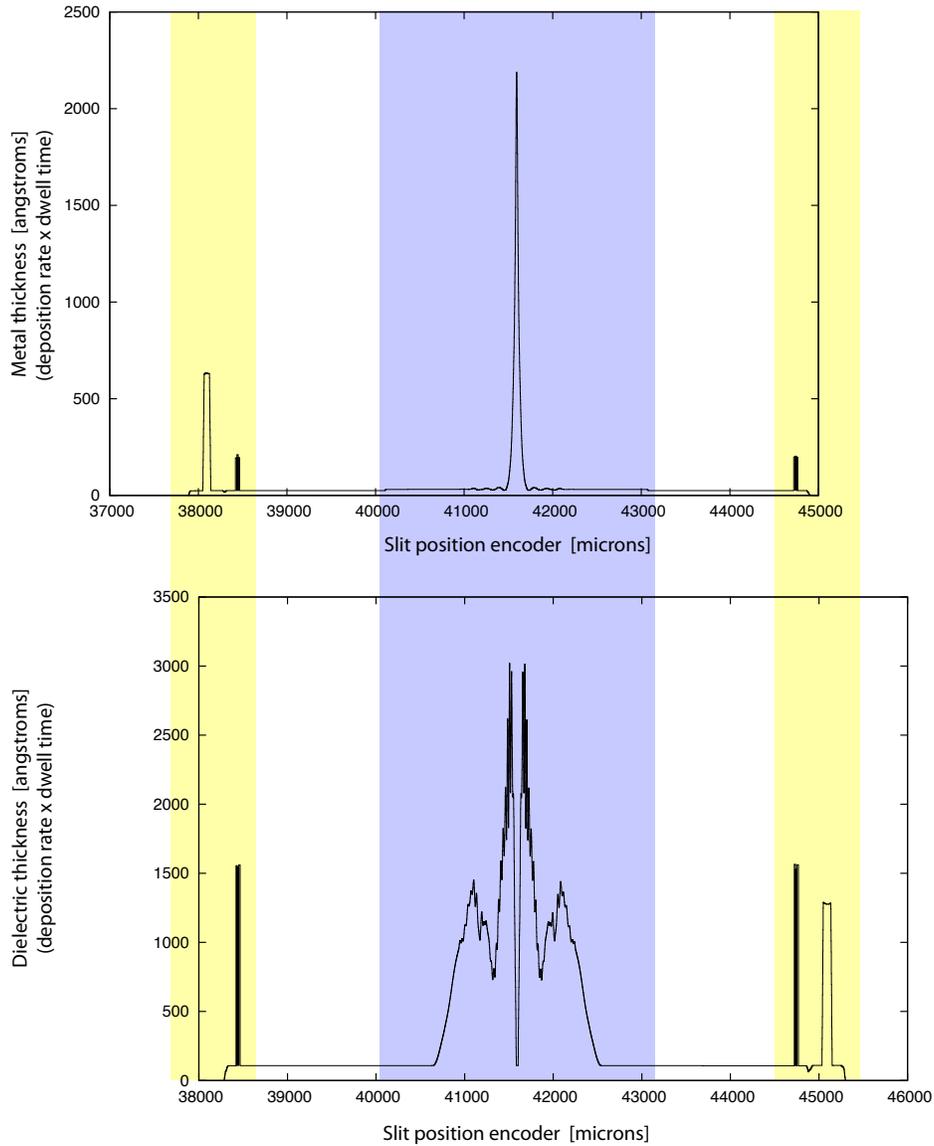
Figure 4. *The deposition process is monitored in real time. These two plots show the thickness profiles, built up as the slit makes 50-60 passes in one-micron steps, each pass incrementally increasing the layer thickness by an amount proportional to the product of deposition rates and dwell times. The plots show the final thicknesses at the completion of the metal deposition (top) and the dielectric deposition (bottom). Highlighted in blue are the active areas of the hybrid Lyot focal plane mask, with a narrowly peaked, nearly band-limited metal profile, and a dielectric profile that tailors the phase shifts in the mask. Highlighted in yellow are the fiducial alignment marks. Also seen are the new thickness calibration features deposited to the left of the pattern in the metal layer, and to the right of the pattern in the dielectric.*

The nickel and cryolite layers of the hybrid Lyot mask are deposited by vacuum evaporation in the facility shown in Figure 3. A slit of 15 μm width, made of silicon with microfabrication techniques at JPL's Micro Devices Laboratory, is mounted close to the fused silica substrate on a computer controlled linear translation stage. The slit, acting as a deposition mask, is scanned across the substrate in 1-micron steps, with dwell times at each step specified to generate the specified thickness profiles. The process is monitored in real time, as indicated in Figure 4. Figure 5 is a photo of a latest mask fabricated to this design. As described later, this hybrid Lyot mask includes both alignment and thickness calibration fiducial marks for improved fidelity of the manufactured mask.
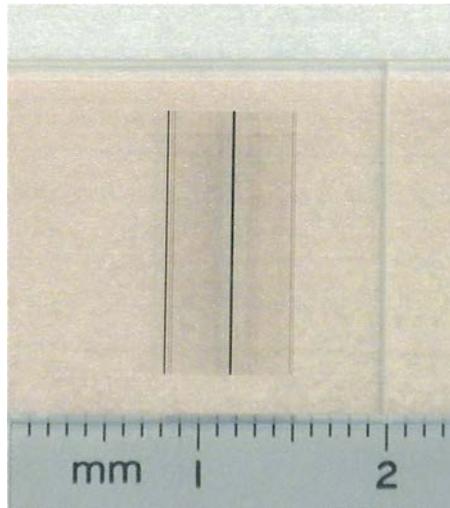
Figure 5. *Photograph of the hybrid Lyot mask, composed of thickness profiled layers of nickel and cryolite superimposed on a fused silica substrate, with a mm scale for comparison. This mask was fabricated in January 2012 with the corrected calibration procedure described in Section 6. The attenuation pattern is clearly seen, including the central peak and fiducial alignment marks to the right and left of center. The new thickness calibration mark for the metal layer is the darker feature seen at the far left. The dielectric calibration mark, at the far right, can only be seen in the phase measuring microscope. Close inspection of these fiducial marks indicate that the slit motions were within one micron of the commanded positions for the entire deposition run, and that the metal and dielectric thicknesses were correct to within thickness measurement errors of five percent. We have since fabricated additional copies of this mask, to this exact prescription, in anticipation of future high contrast coronagraph demonstrations in a 20% bandwidth.*

2.3. HCIT configuration

The optical layout of the HCIT Lyot table during these TDEM experiments is shown in Figure 6. The layout is similar to that proposed in Trauger et al. (2007), with minor modifications. The optical table is operated in the HCIT vibration isolated vacuum chamber that can be evacuated to 10 milliTorr levels.
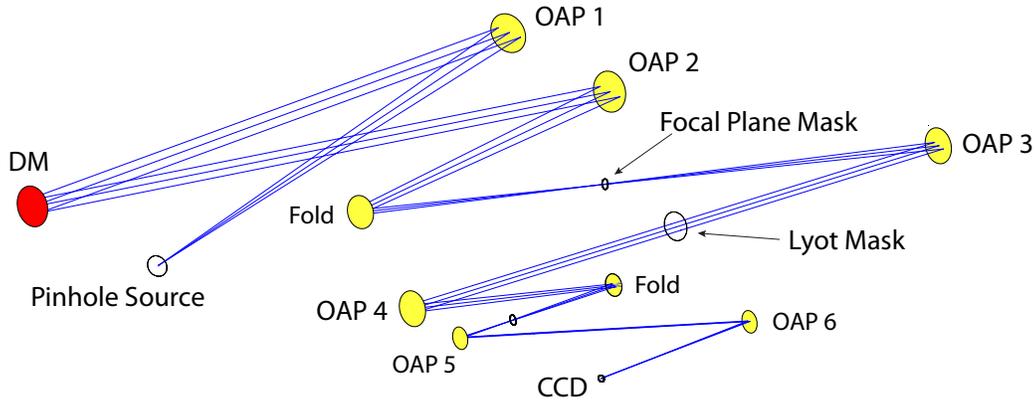
Lyot table – Source-to-occulter alignment history
(Optical path: Zygo–OAP1–DM–OAP2–Fold–Occulter–Retrosphere)
Values are single-pass wavefront (waves @ 633 nm)

	In-air alignment 8/7/09	In HCIT chamber 9/12/09	Realigned 9/16/10
PV =	0.070 ± 0.003	0.087 ± 0.003	0.054 ± 0.003
rms =	0.011 ± 0.001	0.014 ± 0.001	0.008 ± 0.001
0–90° astig =	−0.010 ± 0.002	−0.014 ± 0.002	0.008 ± 0.002
±45° astig =	0.005 ± 0.002	0.000 ± 0.002	−0.005 ± 0.002

Figure 6. *Optical layout and alignment history of the HCIT Lyot coronagraph table. The optical elements in the optical path, starting from the source, are as follows. The source of continuum light illuminates OAP 1, the first of six off-axis paraboloidal (OAP) mirrors, which collimates the beam. The beam passes to the deformable mirror (DM), where a 48 mm diameter aperture stop defines the pupil of the system. The DM is from Xinetics, with a square array of actuators spaced on a 1-mm pitch, such that 1810 actuators are active within the pupil aperture. The collimated light is then focused by OAP 2 and folded by a flat mirror, passing to the focal plane where the hybrid Lyot mask is located. The beam is collimated by OAP 3 on its way to the Lyot stop, which is located in a pupil plane conjugate to the deformable mirror. The collimated beam is then brought to a focus by OAP 4 to create the high-contrast coronagraph image, where a field stop is positioned to reduce scattered light. A camera, formed by OAPs 5 and 6, then magnifies and projects the coronagraph image onto the CCD focal plane. Alignment history, showing only the most critical elements upstream of the focal plane mask, is summarized.*

The simulated "star" in the HCIT is a 5 µm diameter pinhole illuminated by the light from a supercontinuum laser. The supercontinuum source resides outside the vacuum chamber in the ambient laboratory environment. The light emanating from the non-linear supercontinuum fiber is collimated, then passes through a pair of filter wheels populated with up to ten optical bandpass filters. The filters used in this milestone demonstration are high quality multicavity interference filters (from Barr Associates) with square-topped passbands and out-of-band blocking better than 10^{-6}.   The half-transmittance wavelengths are listed in Table 1. The collimated light is then brought to focus at the core

at one end of the 20-meter long single mode transfer fiber, which then passes through a vacuum port into the HCIT chamber. The output of the transfer fiber is again collimated and refocused to pass through the 5 μm source pinhole.

Optical Filter Transmittance Passbands

Filter ID	FWHM wavelength range	Bandwidth ($\delta\lambda/\lambda_o$)
1	719.4 – 735.1 nm	2.2%
2	761.5 – 776.5 nm	2.0%
3	774.7 – 790.1 nm	2.0%
4	790.9 – 806.7 nm	2.0%
5	806.7 – 822.8 nm	2.0%
6	823.1 – 838.6 nm	1.9%
7	864.2 – 879.9 nm	1.8%
8	720.7 – 769.3 nm	6.5%
9	771.5 – 821.2 nm	6.2%
10	823.5 – 878.7 nm	6.5%

Table 1. The set of optical bandpass filters used for these demonstrations. Listed are filter IDs for reference, the spectral passband measured at the half-transmittance wavelengths, and the spectral bandwidth as a percentage of the central wavelength.
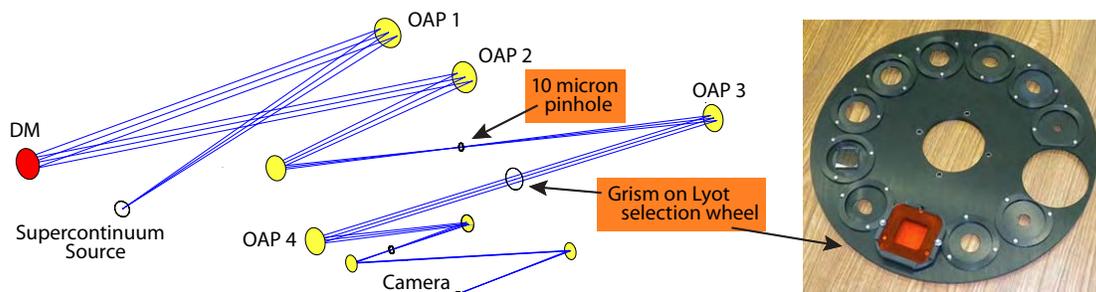
Figure 7. Internal grism mode. Knowledge of the source spectrum is required to certify broadband coronagraph performance. The Lyot coronagraph can be operated as a grism spectrometer for the analysis of the source spectra. A 10-μm diameter pinhole is selected from the array of focal plane masks, and an 8.22 line/mm grism is selected from the array of eleven masks in the Lyot selection wheel (as shown). The spectrum projected on the final CCD focal plane is therefore representative of the end-to-end spectral character of the source.
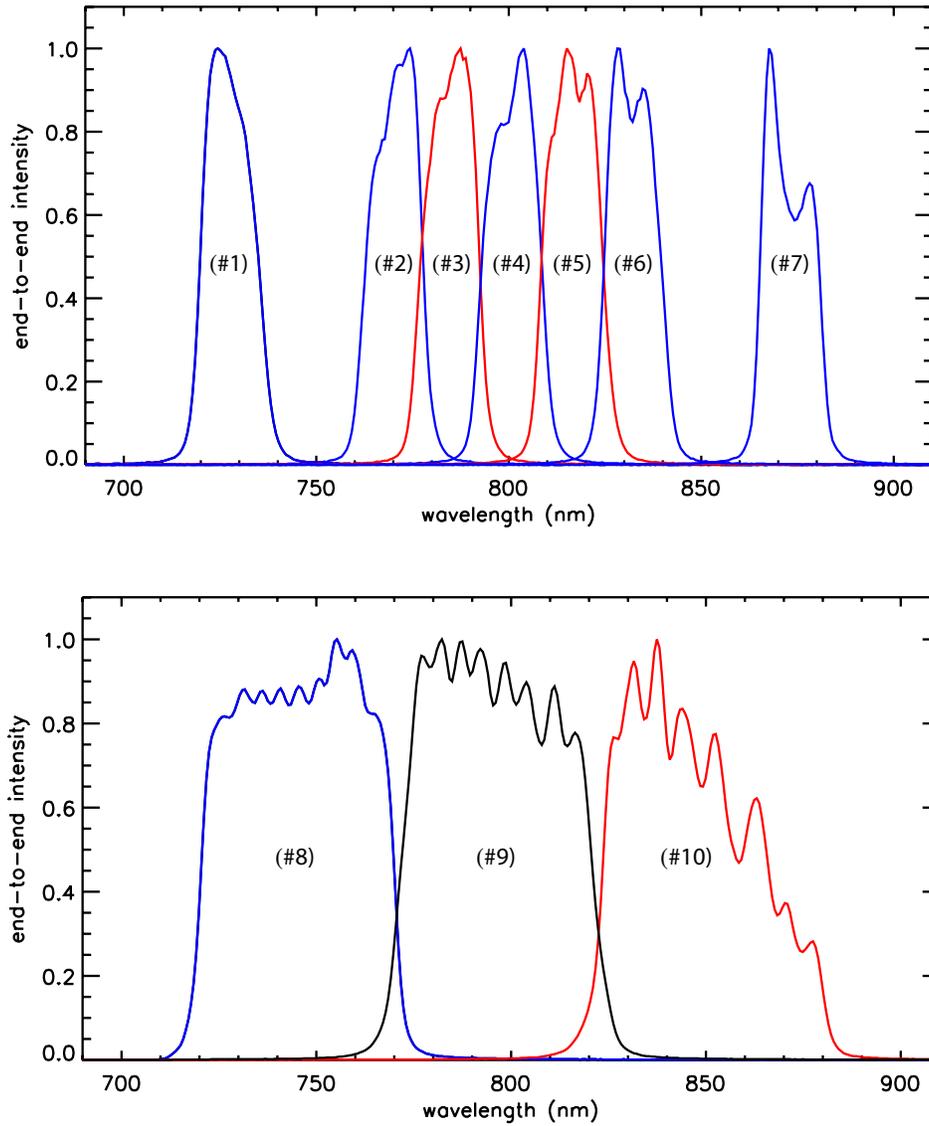
Figure 8. *Grism spectra of the supercontinuum light, as filtered by the ten selectable optical bandpass filters listed in Table 1 and transmitted end-to-end through the coronagraph. An 8.22 lines/mm grism provides a resolving power R = $\lambda/\delta\lambda$ of about 200. The spectrum is dispersed by 0.657 nm/pixel at the CCD focal plane. While all ten multi-cavity interference filters have square-topped transmittance profiles, the end-to-end spectrum is strongly modified, mainly by the intrinsic color of the supercontinuum source and the chromaticism in the lenses coupling the supercontinuum output fiber to the single-mode transfer fiber. In the case of the three contiguous 6.5% filters covering an overall 20% bandpass, we were unable to find an alignment that removed the strong non-uniformity in intensity induced across the #10 passband, which therefore does not fully represent the challenge of a 20% bandwidth.*

The effective spectrum of the "starlight" is critical to the fidelity of our broadband contrast demonstrations. The spectrum is essentially the product of the raw supercontinuum output, the filter profiles, the chromaticity in the lenses that relay the supercontinuum fiber to the transfer fiber and that relay the transfer fiber to the pinhole, the reflectivity of the HCIT mirrors, transmittances of the focal plane mask and CCD window, and the CCD spectral response. Therefore, we must rely on an in situ spectrum measurement to certify that our "starlight" does in fact satisfy the milestone specifications.

We devised a new grism spectrometer mode for the Lyot table, based on an 8.22 line/mm transmission grating on a wedged OG570 glass substrate, mounted in the Lyot selection wheel. The grism dispersion is effectively constant and throughput efficiency is flat across our 720-880 nm wavelength range. Using the x/y/z actuation in the focal plane mask selection stage, a 10-μm pinhole is centered on the star image. The pinhole image is dispersed by the grism, and the spectrum is recorded in the coronagraph CCD. This is illustrated in Figure 7. The grism spectrometer was used to analyze the end-to-end spectral profiles of the supercontinuum source corresponding to each of the ten optical filters, shown in Figure 8.

Coronagraph testbed demonstrations

The milestone demonstrations rely on a wavefront sensing and correction process that has been exercised and validated in previous milestone demonstrations, including TPF-C Milestone #2. A flavor of the "electric field conjugation method" (EFC), as described in Give'on *et al.* (2007), is used and iterated repeatedly as necessary, as follows. For each filter in a set of optical filters that sample the full 20% range of wavelengths, and starting with a nominally flat surface figure setting on the DM: (a) take the set of contrast field images with the initial DM setting and estimate the contrast averaged across the entire 20% band; (b) take images for each of four "probe" DM settings (consisting of small deterministic surface figure deviations from the initial DM setting) to measure the effects of the four probe settings across the entire 20% band; (c) use these data to compute the complex electric field in the target dark field region across the 20% band; and then (d) calculate and apply a new DM setting that will reduce the energy over the dark field in all filters concurrently, thus establishing a new "initial DM setting" in preparation for the next iteration, which is a loop back to step (a). A typical integration time for an individual image is about ten seconds, and one complete wavefront sensing and control cycle, including overhead for CCD readouts, data handling and computations for a 20% band, typically takes 10-15 minutes.

2.4. Differences Between Flight and Laboratory Demonstrations

There are several important differences between the lab demonstration and the ACCESS flight implementation. Each is addressed briefly below.

Starlight: In a space coronagraph, the spectrum of light illuminating the coronagraph would closely resemble black body radiation. The spectral distribution produced by the HCIT light source (a fiber-coupled supercontinuum laser) is smooth, but nevertheless

with variations by up to 50% in brightness vs. wavelength across a 20% spectral band, as is seen in the end-to-end supercontinuum spectra in Figure 8.

As such, a single filter spanning a 20% spectral band will not provide a reliable test of the contrast over the entire spectral band. In our June 2010 White Paper, we proposed to measure the contrast in a set of three contiguous 6.5% passbands that span the full 20% band, and an excellent set of three filters was purchased. The filters are mounted in a selection wheel within the supercontinuum source module outside the vacuum chamber, so that they can be interchanged easily without disrupting the optical system in any way. The measurements in each 6.5% band can be individually calibrated against the photometry reference (as described in Section 3.3) and averaged to construct the contrast metric over the full 20% spectral band. This procedure effectively corrects for the shape, as long as the time scale for variations is long compared to the time for a single wavefront sensing and control iteration.

However, as noted in the caption for Figure 8, we were unable to find an alignment for the longest of the three 6.5% filters that fairly represented a uniform light source at the longest wavelengths in the 20% band, so we decided instead to score the contrast over the the 20% band in five 2% bands. The longest and shortest wavelengths are therefore well represented, and a weighted average with this evenly-spaced picket fence of five passbands provides an accurate estimate of the overall 20% contrast. In this TDEM run, the set of three 6.5% filters were used to demonstrate broadband nulling, while a set of five 2% filters was used to score the final 20% contrast.

The supercontinuum source provides a photon flux that is at least 100 times brighter than the target stars to be observed during the mission (e.g., a star no brighter than visual magnitude V=1 as observed with a 1.5 meter telescope). The goal of this milestone is to demonstrate the broadband contrast that can be achieved, which is independent of the source intensity, so a bright source is a convenience that does not compromise the integrity of the demonstration.

Finally, unlike the light collected by a telescope from a target star, the light is coherent across the 5-μm diameter source pinhole and it projects a slightly non-uniform intensity across the pupil. It is equivalent to a star sufficiently distant to have a negligible angular diameter. Typically the pupil non-uniformity is a center-to-edge "droop" of a few percent corresponding to the diffraction pattern from a 5-μm source pinhole. This small non-uniformity has negligible effect on the final contrast if it is accounted for in the wavefront control algorithm, and would result in a finite but insignificant loss of contrast if it were ignored in the control algorithm.

Spacecraft dynamics: A control system is required in flight to stabilize the light path against motions of the spacecraft. The dominant effects of spacecraft dynamics are jitter of the star image on the coronagraph focal plane mask and beam walk in the optics upstream of the focal plane mask. For a specific example, the ACCESS analysis showed that for fourth-order coronagraphs (including Lyot, vortex, and pupil mapping coronagraphs) with an inner working angle of $3\lambda_o/D$, pointing errors needed to be less than ±0.03 λ_o/D to limit the corresponding contrast degradation to less than 2×10^{-10}. The concept models have shown that the required pointing stability can be achieved in space with current high Technology Readiness Level (TRL) systems. Scaled to the HCIT, this would correspond to an ability to center the occulting mask on the "star" within 1 μm, or about 0.23 pixel when projected to the CCD focal plane.

The milestone demonstration requires the passive stability of the testbed, including the

centration of the star on the occulter as one example, which is untraceable to spacecraft dynamics. In practice, the HCIT often exhibits alignment drifts that are larger than expected in the space environment. As such we must rely on favorable periods of thermal and mechanical stability of the HCIT.

Single deformable mirror: The milestone demonstrations will be carried out with a single DM, which allows the control of phase and amplitude in the complex wavefront over one half of the coronagraph field described in Section 2 above. In flight, it is expected that a pair of DMs will be used, in series, to generate a full (two-sided) dark field, with the added advantages of a deeper contrast field and better broadband control.

3. Computation of the contrast metric

3.1. Definitions

The contrast metric requires a measurement of the intensity of speckles appearing within the dark field, relative to the intensity of the incident star. The contrast metric will be assessed in terms of statistical confidence to capture the impact of experimental noise and uncertainties. In the following paragraphs we define the terms involved in this process, spell out the measurement steps, and specify the data products.

3.1.1. "Raw" Image and "Calibrated" Image. Standard techniques for the acquisition of CCD images are used. We define a "raw" image to be the pixel-by-pixel image obtained by reading the charge from each pixel of the CCD, amplifying and sending it to an analog-to-digital converter. We define a "calibrated" image to be a raw image that has had background bias subtracted and the detector response normalized by dividing by a flat-field image. Saturated images are avoided in order to avoid the confusion of CCD blooming and other potential CCD nonlinearities. All raw images are permanently archived and available for later analysis.

3.1.2. We define "scratch" to be a DM setting in which actuators are set to a predetermined surface figure that is approximately flat (typically, about 20 volts on each actuator).

3.1.3. We define the "star" to be a small pinhole illuminated with broadband light relayed via optical fiber from a source outside the HCIT vacuum wall (e.g., the super-continuum white light source). The "small" pinhole is to be unresolved by the optical system; e.g., a 5-μm diameter pinhole would be "small" and unresolved by the 25-μm FWHM Airy disk in an f/31.25 beam at 800 nm wavelength. This "star" is the only source of light in the optical path of the HCIT. It is a stand-in for the star image that would have been formed by a telescope system.

3.1.4. We define the "algorithm" to be the computer code that takes as input the measured speckle field image, and produces as output a voltage value to be applied to each element of the DM, with the goal of reducing the intensity of speckles.

3.1.5. The "contrast field" is a dimensionless map representing, for each pixel of the detector, the ratio of its value to the value of the peak of the central PSF that would be measured in the same testbed conditions (light source, exposure time, Lyot stop, etc.) if the coronagraph focal plane mask were removed. The calibration of the contrast field is further detailed in Section 3.3.

3.1.6. The "contrast value" is a dimensionless quantity that is the average value of the contrast field over the dark field adopted for the experiment.

3.1.7. "Statistical Confidence". The interpretation of measured numerical contrast values shall take into consideration, in an appropriate way, the statistics of measurement, including detector read noise, photon counting noise, and dark noise.

The milestone objective is to demonstrate with high confidence that the true contrast value in the dark field, as estimated from our measurements, is equal to or better than the required threshold contrast value C_0. The estimated true contrast value shall be obtained from the average of the set of four or more contrast values measured in a continuous sequence (over an expected period of approximately one hour or more).

For this milestone the required threshold is a mean contrast value of $C_o = 1.0 \times 10^{-9}$ with a confidence coefficient of 0.90 or better. Estimation of this statistical confidence level requires an estimation of variances. Given that our speckle fields contain a mix of static and quasi-static speckles (the residual speckle field remaining after the completion of a wavefront sensing and control cycle, together with the effects of alignment drift following the control cycle), that they include the superposition of speckles of multiple wavelengths exhibiting their own deterministic wavelength dependencies, as well as other sources of measurement noise including photon detection statistics and CCD read noise, an analytical development of speckle statistics is impractical. Our approach is to compute the confidence coefficients on the assumption of Gaussian statistics, but also to make the full set of measurement available to enable computation of the confidence levels for other statistics. One data product will be a goodness of fit of the measurement with a normal distribution (Kolmogorov-Smirnov test).

At any time in the demonstration, the true contrast is subject to laboratory conditions, including the quality of the optical components, their alignment, any drift in their alignment over time, and the effectiveness of each wavefront sensing and control cycle. With each iteration, our nulling procedure attempts to improve the contrast value, thus compensating for any drift or changes in alignment that may have occurred since the previous iteration, and further variations may be expected due to experimental noise and any limitations in the algorithm. The data set built up from a sequence of such iterations will provide a distribution of contrast values, which will be regarded as Gaussian about a mean contrast for the data set. We therefore consider the mean contrast value as representative of the true contrast value for a data set, and the distribution of contrast determinations among the iterations within the data set as a combination of both random wavefront control errors and random measurement errors.

The mean contrast values and confidence limits are computed in the following manner. The average of one or more images taken at the completion of each iteration is used to compute the contrast value c_i. The mean contrast for a set of images taken in a given sequence is:

$$\hat{c} = \sum_{i=1}^{n} \frac{c_i}{n}$$

where n is the number of images in each set. The standard deviation σ_{each} in the contrast values c_i obtained for individual images within the set, which now includes both the measurement noise and the (assumed random) contrast variations due to changes in the DM settings for each speckle nulling iteration, is:

$$\sigma_{each} = \sqrt{\sum_{i=1}^{n} \frac{(c_i - \hat{c})^2}{n-1}}$$

Our estimate $\hat{c}$ is subject to uncertainty in the contrast measurements $\sigma_{mean} = \sigma_{each} / \sqrt{n}$ and the independently-determined overall errors in photometry σ_{phot}. With the approximation that the contrast values have a Gaussian distribution about the mean contrast, then the statistical confidence that the mean contrast is less than $Co = 1.0 \times 10^{-9}$ is given by:

$$conf = \frac{1}{\sqrt{2\pi}} \int_{-\infty}^{t} e^{-z^2/2} dz$$

where $t = (C_0 - \hat{c})/\sigma$ and $\sigma = \sqrt{\sigma_{mean}^2 + \sigma_{phot}^2}$. The values $\hat{c}$ and σ are the milestone metrics. The 90% confidence value is the value Co such that $conf(Co) = 0.9$ according to the above equations.

3.2. Measurement of the Star Brightness

The brightness of the star is measured with the following steps.

3.2.1. The occulting mask is laterally offset, so as to place a transparent region in its transmittance profile at the location of the star image. The transmittance profile of the occulting mask is known from imaging data from a microscope CCD camera.

3.2.2. To create the photometric reference, a representative sample of short-exposure (e.g. a few milliseconds) images of the star is taken, with all coronagraph elements other than focal-plane occulting mask in place.

3.2.3. The images are averaged to produce a single star image. The "short-exposure peak value" of the star's intensity is estimated. Since the star image is well-sampled in the CCD focal plane (the Airy disk is sampled by ~20 pixels within a radius equal to the FWHM), the star intensity can be estimated using either the value of the maximum-brightness pixel or an interpolated value representative of the apparent peak.

3.2.4. The "peak count rate" (counts/sec) is measured for exposure times of microseconds to tens of seconds.

3.3. Measurement of the Coronagraph Contrast Field

Each "coronagraph contrast field" is obtained as follows:

3.3.1. The occulting mask is centered on the star image.

3.3.2. An image (typically exposure times of ~tens of seconds) is taken of the coronagraph field (the suppressed star and surrounding speckle field). The dimensions of the target areas, as shown schematically in Figure 4, are defined as follows: (a) A dark outer (D-shaped) field extending from 3 to 15 $\lambda o/D$, representing a useful search space, is bounded by a straight line that passes 3 $\lambda o/D$ from the star at its closest point, and by a circle of radius 10 $\lambda o/D$ centered on the star. (b) An inner area within the foregoing dark field, representing contrast at the inner working angle of 3 $\lambda o/D$, is bounded by a square

box, each side measuring $\lambda o/D$, such that one side is coincident with the foregoing straight line and centered on the closest point to the star.
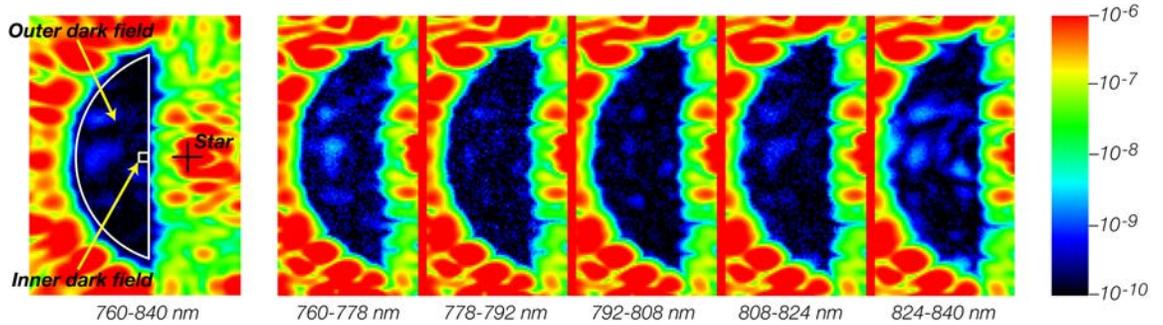

Figure 9. *Definition of the high-contrast dark field. As described in the text, inner and outer regions are defined for the one-sided dark field. The location of the suppressed central star is also indicated. Adapted from Moody et al. (2008), this shows the dark field averaged over a 10% bandwidth (at left), and the five individual 2% dark fields (at right), corresponding to the TPF-C Milestone 2 demonstration.*

3.3.3. The image is corrected for the attenuation profile of the occulter and normalized to the "star brightness" as defined in 3.2. For this purpose, the fixed relationship between peak star brightness and the integrated light in the speckle field outside the central DM-controlled area will be established, as indicated in Figure 10 (taken from TPF-C Milestone Report #1, Trauger et al. 2006), providing the basis for estimation of star brightness associated with each coronagraph image.
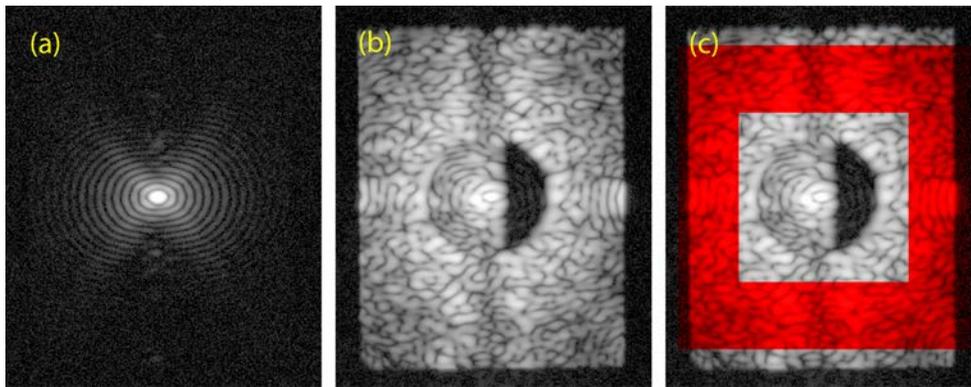
Figure 10. *Reference fields for contrast photometry. Shown here are (a) the "planet" reference image; (b) the high-contrast coronagraph field; and (c) superimposed in red is the reference speckle field in the "uncontrolled" area beyond the Nyquist limit for the deformable mirror. Images are displayed with a logarithmic contrast stretch.*

3.3.4. The contrast field image is averaged over the target high-contrast areas, to produce the contrast value. In the case of multiple filters used to represent the full bandwidth (e.g., five 2% filters across a 20% overall spectral band), the contrast is the average of contrasts obtained over the full set of filters for a single setting of the DM. To

18

be explicit, the contrast value is the sum of all contrast values, computed pixel-by-pixel in the dark field area, divided by the total number of pixels in the dark field area, without any weighting being applied. In the case of multiple filters representing the full bandwidth, the overall contrast is the average of contrasts calibrated and estimated individually for each of the passbands. This effectively creates a star spectrum that is flat in units of photon counts / nm / second. The rms contrast in a given area is calculated from the same contrast field image.

3.4. Milestone Demonstration Procedure

The procedure for the milestone demonstration is as follows:

3.4.1. As mentioned above, we have used a set of five 2% FWHM filters to represent the 20% spectral band. The DM is set to scratch. An initial coronagraph contrast field image is obtained for each of the five filters, as described in Sec. 3.3.

3.4.2. Wavefront sensing and control is performed to find settings of the DM actuators that give the required high-contrast across the 20% band in the target dark field. This iterative procedure may take several hours, starting from scratch, if no prior information is available.

3.4.3. Subsequent contrast field images are taken, in each of the five filters, following steps 3.3.1 – 3.3.4, at the rate of about four contrast field images per hour, for a period of at least one hour. The result at this point is a set of contrast field images representing the full 20% spectral band. It is required that a sufficient number of images are taken to provide statistical confidence that the milestone contrast levels have been achieved, as described in Section 3.1.7 above.

3.4.4. Laboratory data are archived for future reference, including raw and calibrated images of the reference star and contrast field images.

4. Success criteria

The following are the required elements of the milestone demonstration. Each element includes a brief rationale.

4.1. A set of five optical filters with 2% passbands, shall be used to sample the full 720–880 nm FWHM wavelength range. Contrast values estimated in each of these filters for a single DM setting shall be averaged to determine the broadband contrast.

Rationale: *As described in Section 2.3, this approach is required to correct for spectral variations in the supercontinuum light source, a problem that will not be encountered with real stars in a space mission.*

4.2. A mean contrast metric of 1×10^{-9} or better shall be achieved in both an outer target dark area ranging from 3 to 15 λ_o/D and an inner area ranging from 3 to 4 λ_o/D, as defined in Sec. 3.3.2.

Rationale: *The outer area provides evidence that the high contrast field provides a useful search space for planets. The inner area tests for fundamental limitations at the inner working angle.*

4.3. Criteria 4.1 and 4.2, averaged over the data set, shall be met with a confidence of 90% or better, as defined in Sec. 3.1.7. Sufficient data shall be taken to justify this statistical confidence. It is expected that this confidence level can be met with a data set taken as a single sequence of images over a period of one hour or more. This criterion is deemed to have been met by a data set exhibiting the stated statistical confidence.

Rationale: *This milestone is intended to validate the ability of the hybrid mask technology to deliver the contrast and bandwidth performance specified in Section 2. The mask itself is a passive element of the coronagraph, constructed with the same methods and materials used for optical filters that have flown in space for decades, with optical characteristics that can be considered permanent and insensitive to the environmental influences of a space mission. As such, a statistically significant measurement of achieved coronagraph contrast establishes the capability of the mask.*

4.4 The demonstration described in 4.3 will be repeated on three separate occasions, with different masks used on each occasion. In this context a different mask is deemed to be either a different section of a linear mask separated by an angle of at least 3 λ_o/D, or a physically separate mask.

Rationale: *Because the milestone is directed at a component test, the component must change between tests, but it is not required that the software control system be reset between each demonstration. This is to say that for each demonstration, the DM need not begin from a "scratch" setting and the DM control algorithm may retain memory of settings used for prior demonstrations. There is no time requirement for the demonstrations, other than the time required to meet the statistics stipulated in success criterion 4.3. There is no required interval between demonstrations. Subsequent demonstrations can begin as soon as prior demonstration has ended. There is no requirement to turn off power, open the vacuum tank, or delete data relevant for the calibration of the DM response functions.*

5. Experimental results

Here we collect nine data sets representative of the experimental results of our 12-week HCIT run in May-July 2011. These each include measured contrast for six consecutive iteration cycles, sufficient to establish a statistically significant result. We include the following data sets.

Data set 1. Contrast demonstration in a single 2% band centered at 800 nm (Filter 4) is shown in Table 2. This narrowband series establishes the limiting contrast for the system including both incoherent scattered background and unsuppressed coherent starlight, with a minimum of spectral bandwidth and chromatic effects. The average contrast in the inner 3-4 λ_o/D field is 3.42 ($\pm$ 0.05) $\times 10^{-10}$, while the average in the outer 3-15 λ_o/D field is 2.25 ($\pm$ 0.03) $\times 10^{-10}$. The mean contrast is better than 1×10^{-9} with a confidence level > 99%.

Narrowband 800 nm contrast demonstration with a single 2% filter

Date & Time	Inner Field ($\times 10^{-9}$)	Outer Field ($\times 10^{-9}$)
16 Jul 2011 – 13:07	0.401	0.227
16 Jul 2011 – 13:19	0.317	0.226
16 Jul 2011 – 13:31	0.381	0.224
16 Jul 2011 – 13:43	0.327	0.225
16 Jul 2011 – 13:55	0.271	0.229
16 Jul 2011 – 14:07	0.353	0.221

Table 2. Raw contrast measurements in narrowband light. Dark field nulling was carried out with a single 2% filter centered at a wavelength of 800 nm. Listed are the raw contrasts measured in the inner and outer fields for six consecutive nulling iterations.

Data sets 2,3,4. Contrast over a 10% band was obtained in five contiguous 2% spectral bands (Filters 2,3,4,5,6), in a manner nearly identical to that of TPF-C Milestone #2. We have selected three sets of six nulling cycles each, with results collected in Table 3. Each set was taken at a different position on the same linear Lyot mask, with the location of the star along the occulter shifted from the others by more than 3 λ_o/D. The average contrast in the inner 3-4 λ_o/D field is 6.72 ($\pm$ 1.58) $\times 10^{-10}$, while the average in the outer 3-15 λ_o/D field is 6.14 ($\pm$ 0.67) $\times 10^{-10}$. The mean contrast is better than 1×10^{-9} with a confidence level > 98%.

Data sets 5,6,7. Contrast over a 20% band was obtained in five 2% spectral bands (Filters 1,2,4,6,7) spanning 720-880 nm. We have selected three sets of six cycles each, with results collected in Table 4. Each set was taken at a different position on the same linear Lyot mask, with the location of the star on the occulter shifted from the others by

more than 3 λ_o/D. The average contrast in the inner 3-4 λ_o/D field is 2.30 ($\pm$ 0.30) $\times10^{-9}$, while the average in the outer 3-15 λ_o/D field is 1.79 ($\pm$ 0.16) $\times10^{-9}$.

Data set 8. A contrast demonstration in a single 6.2% band (Filter 9) centered at 800 nm is shown in Table 5. Both nulling and contrast scoring were carried out with just this single filter, demonstrating high contrast wavefront control in a spectral band significantly larger than 2% and indicating that our wavefront sensing and control model has successfully accounted for chromatic effects at the demonstrated contrast level. The average contrast in the inner 3-4 λ_o/D field is 5.85 ($\pm$ 0.66) $\times10^{-10}$, while the average in the outer 3-15 λ_o/D field is 4.25 ($\pm$ 0.21) $\times10^{-10}$. The mean contrast is better than 1×10^{-9} with a confidence level > 99%.

Data set 9. Contrast over a 20% band was demonstrated in three 6.5% filters (Filters 8,9,10) as listed in Table 6, with the caveat that the longest wavelengths in the 720-880 nm band are somewhat underrepresented (due to a non-uniform supercontinuum spectrum in Filter 10) when averaging the contrast in all three spectral bands. The average contrast in the inner 3-4 λ_o/D field is 1.84 ($\pm$ 0.35) $\times10^{-9}$, while the average in the outer 3-15 λ_o/D field is 1.72 ($\pm$ 0.11) $\times10^{-9}$. This data set demonstrates that the chromatic effects across the 6.5% spectral bands are sufficiently well represented in our model to support broadband nulling with results comparable to the earlier nulling in 2% bands, setting the stage for highly efficient dark field nulling in the future with single filters as broad as 20%.

Contrast over a 10% spectral band with 5 × 2% FWHM filters

Occulter y-coordinate = 2.270 mm

Date & Time	Inner Field (×10^{-9})	Outer Field (×10^{-9})
16 Jul 2011 – 5:03	0.610	0.519
16 Jul 2011 – 5:32	0.654	0.523
16 Jul 2011 – 6:02	0.620	0.520
16 Jul 2011 – 6:32	0.562	0.520
16 Jul 2011 – 7:03	0.564	0.522
16 Jul 2011 – 7:33	0.662	0.523

Occulter y-coordinate = 1.270 mm

Date & Time	Inner Field (×10^{-9})	Outer Field (×10^{-9})
26 Jul 2011 – 7:51	0.986	0.660
26 Jul 2011 – 8:18	0.971	0.664
26 Jul 2011 – 8:44	0.658	0.656
26 Jul 2011 – 9:11	0.815	0.654
26 Jul 2011 – 9:39	0.831	0.665
26 Jul 2011 – 10:14	0.914	0.669

Occulter y-coordinate = 0.350 mm

Date & Time	Inner Field (×10^{-9})	Outer Field (×10^{-9})
28 Jul 2011 – 15:23	0.544	0.663
28 Jul 2011 – 15:55	0.573	0.662
28 Jul 2011 – 16:27	0.539	0.655
28 Jul 2011 – 17:43	0.569	0.651
28 Jul 2011 – 18:19	0.513	0.665
28 Jul 2011 – 18:51	0.516	0.653

Table 3. *Raw contrast measurements across a 10% spectral bandwidth. Dark field nulling was carried out using five filters with contiguous 2% passbands spanning the 760-840 nm spectral range. Listed are the measured contrasts in the inner field (a square box extending from 3 to 4 λ_o/D) and averaged over an outer field (extending to a radius of 15 λ_o/D) for six consecutive nulling iterations. The three sets of data are taken at different positions along the linear focal plane mask. Offset between the set at top and at center is 1.00 mm = 40 λ_o/D. The set at bottom is displaced by an additional 0.92 mm = 37 λ_o/D.*

Contrast over a 20% spectral band with 5 × 2% FWHM filters

Occulter y-coordinate = 2.270 mm

Date & Time	Inner Field ($\times 10^{-9}$)	Outer Field ($\times 10^{-9}$)
11 Jul 2011 – 20:23	2.35	1.84
11 Jul 2011 – 20:48	2.15	1.83
11 Jul 2011 – 21:13	2.57	1.82
11 Jul 2011 – 21:38	2.47	1.79
11 Jul 2011 – 22:04	2.44	1.83
11 Jul 2011 – 22:29	2.28	1.83

Occulter y-coordinate = 1.270 mm

Date & Time	Inner Field ($\times 10^{-9}$)	Outer Field ($\times 10^{-9}$)
25 Jul 2011 – 21:53	2.68	1.63
25 Jul 2011 – 22:25	2.51	1.61
25 Jul 2011 – 22:56	2.60	1.62
25 Jul 2011 – 23:28	2.60	1.57
26 Jul 2011 – 0:00	2.50	1.54
26 Jul 2011 – 0:32	2.65	1.52

Occulter y-coordinate = 0.350 mm

Date & Time	Inner Field ($\times 10^{-9}$)	Outer Field ($\times 10^{-9}$)
28 Jul 2011 – 5:30	1.97	1.97
28 Jul 2011 – 5:58	1.82	1.94
28 Jul 2011 – 6:26	1.89	1.95
28 Jul 2011 – 6:55	1.92	1.93
28 Jul 2011 – 7:23	2.09	1.96
28 Jul 2011 – 7:51	1.92	1.97

Table 4. *Raw contrast measurements across a 20% spectral bandwidth. Dark field nulling was carried out using five filters 2% spaced across the 720-880 nm spectral range. Listed are the measured contrasts in the inner field (a square box extending from 3 to 4 λ_o/D) and averaged over an outer field (extending to a radius of 15 λ_o/D) for six consecutive nulling iterations. The three sets of data are taken at different positions along the linear focal plane mask. Offset between the set at top and at center is 1.00 mm = 40 λ_o/D. The set at bottom is displaced by an additional 0.92 mm = 37 λ_o/D.*

Contrast demonstration with a single 6.5% FWHM filter

Date & Time	Inner Field ($\times 10^{-9}$)	Outer Field ($\times 10^{-9}$)
9 Aug 2011 – 5:23	0.575	0.508
9 Aug 2011 – 5:30	0.522	0.507
9 Aug 2011 – 5:37	0.494	0.509
9 Aug 2011 – 5:43	0.637	0.512
9 Aug 2011 – 6:00	0.632	0.515
9 Aug 2011 – 6:17	0.650	0.505

Table 5. *Dark field nulling was carried out with a single 6.5% filter spanning the 772–821 nm wavelength range. Listed are the measured contrasts in the inner and outer fields for six consecutive nulling iterations. Contrast performance matches that in the 10% demonstration (Table 2), but in a single filter that gathers more photons/second than a comparable set of three 2% filters, for a quicker nulling sequence as would be desired in a space mission where calibration time and stellar flux are limited.*

Contrast over a 20% spectral band with $3 \times 6.5\%$ FWHM filters

Date & Time	Inner Field ($\times 10^{-9}$)	Outer Field ($\times 10^{-9}$)
8 Aug 2011 – 5:20	1.84	1.72
8 Aug 2011 – 5:34	1.84	1.71
8 Aug 2011 – 5:48	1.86	1.70
8 Aug 2011 – 6:01	1.87	1.72
8 Aug 2011 – 6:15	1.85	1.73
8 Aug 2011 – 6:29	1.77	1.71

Table 6. *Dark field nulling was carried out using three filters with contiguous 6.5% passbands spanning the 720-880 nm spectral range. Listed are the measured contrasts in the inner field (a square box extending from 3 to 4 λ_o/D) and averaged over an outer field (extending to a radius of 15 λ_o/D) for six consecutive nulling iterations. Broad spectral bands (that gather more photons/second distributed among fewer filters) enable a quicker nulling sequence, as would be desired in a space mission where calibration time and stellar flux are limited.*

6. Analysis and fabrication improvements

Based on past experiments on the HCIT, we expect good agreement between the measured (Tables 2 through 6) and predicted (Figure 2 and its caption) coronagraph contrast. Given our evident disagreement, we undertook a number of empirical investigations of the most likely possible causes for our disagreement during our May-

July 2011 run. Several lines of evidence led us to conclude that the Lyot mask had been fabricated with a large calibration error for the dielectric thickness. As indicated in Figure 4 and the surrounding text, the thicknesses of the individual metal and dielectric layers are monitored during deposition with a quartz crystal microbalance. A calibration factor is needed to relate the thickness deposition rates on the crystal monitor and the occulter substrate. An error in these calibration factors would lead to a metal or dielectric layer that systematically differs from the target thickness profiles by a constant of proportionality. We used our models to predict the effects of errors in the calibration factors for either the metal or dielectric films, under the same constraints as the testbed nulling experiment, and were quickly led to suspect that the calibration factor for the dielectric layer was in error by as much as 20%. One of these lines of evidence is shown in Figure 11.
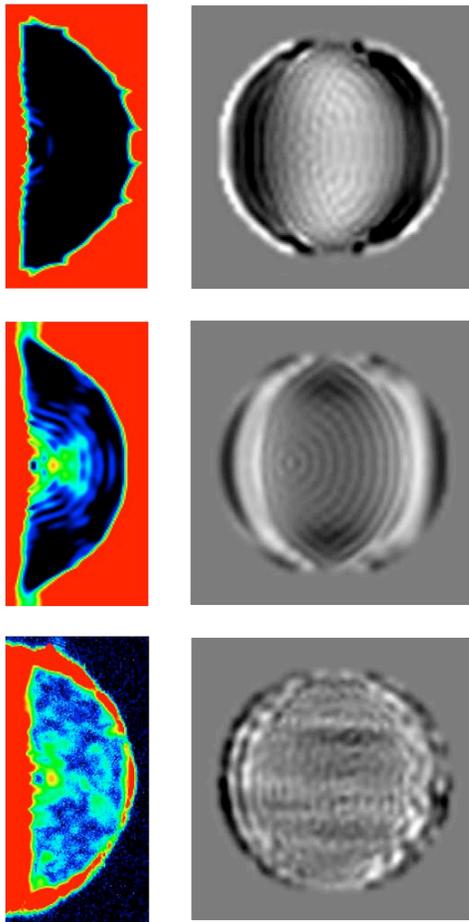

Figure 11. Comparison of predicted 20% bandwidth performance for a correctly fabricated Lyot mask (top); with a Lyot mask with 20% deficit in the dielectric layer (center); and with experimental results as obtained during the May-July 2011 HCIT run (bottom). The predicted dark field and DM settings for the perfect mask are identical to those shown in Figure 1 (but reversed right-left). The three dark field images and DM surface figure settings are each displayed with the same contrast stretch to facilitate direct comparisons. We note that a distinctive pair of dark and bright speckles appears in the dark fields. They are centered vertically near the inner edge in the center and bottom images. Furthermore, the DM settings for the center and bottom images are approximately reversed (hills vs. valleys on the DM surface) compared to the perfect case at top. This signature indicated that a deficit in dielectric thickness was a likely cause of our failure to reach the predicted 20% contrast. This indication was confirmed by inspection of the fabrication hardware.

Our suspicion was confirmed by microscope inspection of the 15-micron slit used for the mask deposition. The width of the slit narrowed significantly during the dielectric deposition due to buildup of the material on the sides of the slit, as can be seen in Figure 12 below.

We have revised our calibration and fabrication process to ensure that this particular problem will not recur in future work, as follows. (1) A calibration pattern, consisting of 100 μm-wide bars of cryolite of various thicknesses between 5 and 200 nm, are deposited

on a fused silica substrate with a new 15-µm slit and the same deposition setup. In order to replicate the narrowing effects shown in Figure 12, we have added additional cryolite features to the pattern that require the full measure of cryolite specified for the actual Lyot mask, rather than a minimal amount used in earlier calibrations. (2) We have found that final cleaning of the slit in an oxygen plasma asher gives much improved adhesion of the metal to the slit, thus eliminating separation of the nickel layer from the slit during thermal cycles in the deposition process, which formerly led to unpredictable variations in the slit clearance. (3) We have added thickness calibration "witness bars" to the deposition pattern (as indicated in Figures 4 and 5) to allow measurement and verification of the correct thickness factors after-the-fact in the finished Lyot mask.

These steps have been taken to ensure that the narrowing effect is repeatable and representative of the overall fabrication process. A new mask was fabricated with the improved calibration in January 2012. We expect to fabricate a few additional masks as time permits, in preparation for a possible future high contrast run in the HCIT.
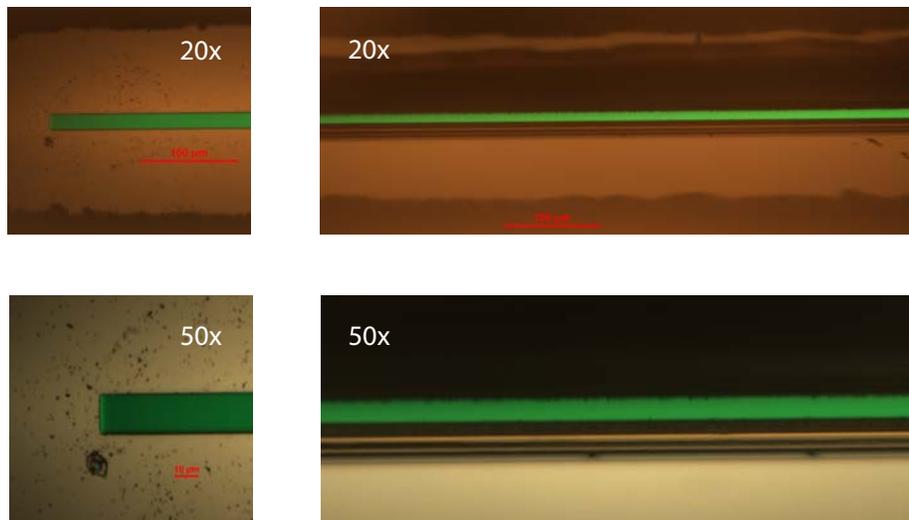

Figure 12. Microscope images of the 15-µm slit used for the vacuum deposition of the Lyot mask in our May–July 2011 HCIT run. Green hues indicate light transmitted through the slit, brown hues indicate light reflected from the slit. At top left, at 20× magnification, is one end of the slit that was shielded and therefore received no material deposition, showing the full 15 µm width. At top right is the appearance near the middle of the slit, showing a reduction in width in the location of the mask deposition. These same areas are imaged at 50x magnification at bottom. Further analysis indicates that the buildup of dielectric has narrowed the slit to approximately 58% of its initial width upon the completion of the deposition, leading to an average ~21% deficit in the thickness of the dielectric layer. This problem has been corrected by carrying out a new calibration that accounts for the full buildup and narrowing of the slit. A new mask has been fabricated with this calibration correction and is ready for a future run in the HCIT (Figures 4 and 5).

7. Certification – deferred

As the formal 20% milestone was not met during our May-July 2011 HCIT run, we will defer the certification process to a future time following a successful run with a corrected hybrid Lyot mask. At that time, the TDEM team will assemble a milestone certification data package for review by the ExEPTAC and the ExEP program. In the event of a consensus determination that the success criteria have been met, the project will submit the findings of the review board, together with the certification data package, to NASA HQ for official certification of milestone compliance.

7.1. Milestone Certification Data Package

The milestone certification data package will contain the following explanations, charts, and data products.

5.1.1. A narrative report, including a discussion of how each element of the milestone was met, and a narrative summary of the overall milestone achievement.

5.1.2. A description of the optical elements and their significant characteristics.

5.1.3. A tabulation of the significant operating parameters of the apparatus.

5.1.4. A calibrated image of the reference star, and the photometry method used.

5.1.5. Calibrated images of the Lyot mask transmittance pattern.

5.1.6. Spectrum of the broadband light and an estimate of the intensity uniformity of the illumination reaching the defining pupil (at the DM).

5.1.7. A contrast field image representative of the data set, with appropriate numerical contrast values indicated, with coordinate scales indicated in units of Airy distance (λ_o/D).

5.1.8. A description of the data reduction algorithms, in sufficient detail to guide an independent analysis of the delivered data.

5.1.9. Contrast metric values and supporting statistics for the overall data used to satisfy the milestone requirements, including a pixel-by-pixel histogram of contrast values across the dark field.

8. New circular Lyot mask designs

As one of the overall goals stated in our hybrid Lyot TDEM proposal, we continue to explore the design space for hybrid Lyot masks, looking for better performance, while using the same integrated design software package as for the linear mask described above. We have begun an investigation of high performance circular Lyot masks with inner working angles as small as 2.5 $\lambda o/D$ and spectral bandwidths greater than 18%.
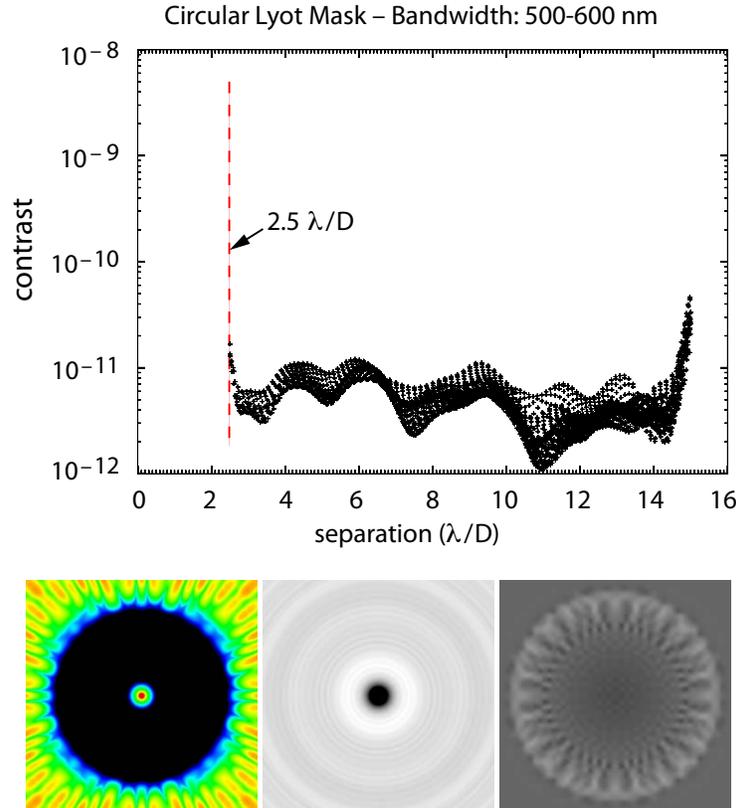

Figure 13. *Predicted performance for a newly designed circular hybrid Lyot mask. Inner working angle is 2.5 $\lambda o/D$. As for the linear mask design, the thickness profiles of the metal and dielectric layers are adjusted in concert with the wavefront control enabled by a single 48×48 DM. Note that a full 360° dark field has been created with a single deformable mirror. Contrast in the 500-600 nm ($\delta\lambda/\lambda o = 18\%$) spectral band is 5.3×10^{-12} in both the inner 2.5-3.5 $\lambda o/D$ annulus and averaged across the entire dark field extending from radii of 2.5 to 15 $\lambda o/D$. The three images at bottom are: (left) the high contrast dark field displayed on a logarithmic contrast stretch from 10^{-11} to 10^{-7}, (center) the intensity transmittance of the occulting mask on a linear scale from 0 to 1, and (right) the DM setting on a black-to-white linear scale of ±75 nm surface displacement.*

We present three examples, all designed for a 2.5 $\lambda o/D$ inner working angle, with bandwidths of 18, 24, and 27% centered on $\lambda o = 550$ nm. Figure 13 illustrates a design that provides contrast better than 1×10^{-11} over the entire dark field extending from 2.5 to

15 λ_o/D, and over the 500–600 nm wavelength band. Further, we note that this full dark field can be achieved with relatively small strokes of a single 48×48 actuator DM by exploiting the ability of a DM to control the real and imaginary parts of the complex wavefront over half the controllable area (in this case, the central half, rather than the right or left half). Figures 14 and 15 illustrate design solutions for larger bandwidths. Both of these designs provide contrasts better than 1×10^{-9} over the entire dark field. The fabrication of these designs will be pursued as opportunities arise in the future.
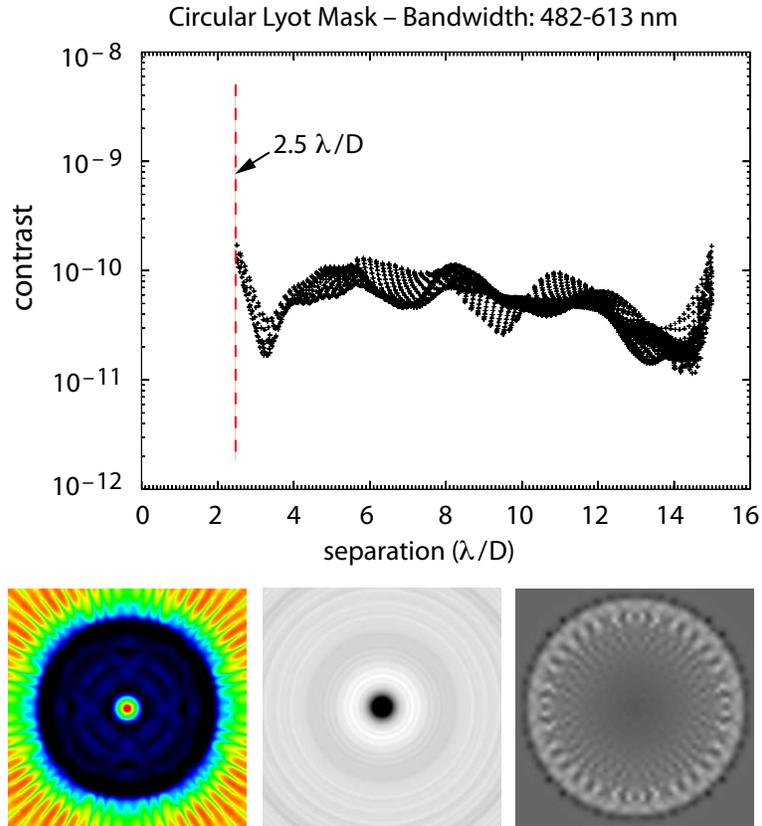

Figure 14. *Predicted performance for a newly designed circular hybrid Lyot mask. Inner working angle is 2.5 λ_o/D. This design extends the design shown in Figure 13 to a larger bandwidth. The thickness profiles of the metal and dielectric layers are adjusted in concert with the wavefront control enabled by a single 48×48 DM. Note that a full 360° dark field has been created with a single deformable mirror. Contrast in the 482-613 nm ($\delta\lambda/\lambda_o$ = 24%) spectral band is 5.2×10^{-11} in both the inner 2.5-3.5 λ_o/D annulus and averaged across the entire dark field extending from radii of 2.5 to 15λ_o/D. For comparisons with Figure 13 above, the three images at bottom are displayed with the same contrast levels as in Figure 13. We note that this larger bandwidth requires larger DM deflections than the 18% case above.*
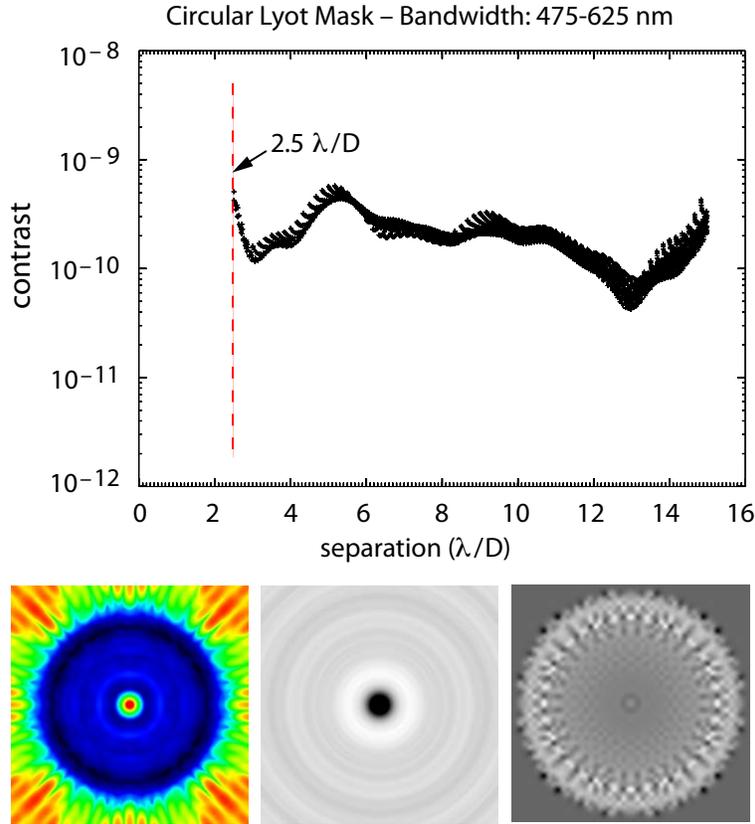
Circular Lyot Mask – Bandwidth: 475-625 nm

Figure 15. *Predicted performance for a newly designed circular hybrid Lyot mask. Inner working angle is 2.5 λ_o/D. This design extends the design shown in Figure 13 to a still larger bandwidth, while sacrificing limiting contrast. The thickness profiles of the metal and dielectric layers are adjusted in concert with the wavefront control enabled by a single 48×48 DM. Note that a full 360° dark field has been created with a single deformable mirror. Contrast in the 475-625 nm ($\delta\lambda/\lambda_o = 27\%$) spectral band is 1.9×10^{-10} in both the inner 2.5-3.5 λ_o/D annulus and averaged across the entire dark field extending from radii of 2.5 to 15 λ_o/D. For comparisons with Figure 13 above, the three images at bottom are displayed with the same contrast levels as in Figure 13. We note that this still larger bandwidth requires larger DM deflections than the 24% case above.*

9. Conclusions and lessons learned

This TDEM program has provided an opportunity for significant progress in the design and fabrication of a coronagraph flight instrument. While we fell short of the stated goal, we have demonstrated raw imaging contrast that exceeds all other published results we are aware of at 3 λ_o/D inner working angles over spectral bandwidths of 2, 6.5, 10, and 20%. The TDEM experience has allowed us to upgrade our design and fabrication process, and has proven the value of a seamless software approach that encompasses mask design, wavefront sensing and control, optical tolerancing and diagnostics, and real-time testbed control. We have corrected our fabrication processes and have produced a

new hybrid Lyot mask for testbed opportunities that may arise in the future, with full expectations that it will perform at the contrast levels defined for this milestone. And we have embarked on the design of circular hybrid Lyot masks that promise ultimately better performance and efficiency compared to the linear masks in this report. Our experience has opened new avenues for future progress, and we are optimistic that significant further advances will follow. We pass along a number of lessons learned in this experience.

1. Clearly, the main lesson learned in this experiment has to do with a correction in the calibrations for the fabrication processes, and steps have been take to mitigate this particular problem in the future. We have fabricated a corrected hybrid Lyot mask based on the same linear hybrid design, and therefore we expect to see the predicted performance illustrated in Figure 2.

2. Nulling demonstrations in 6.5% bandwidths were successful, but our 20% result was compromised in part by non-uniform intensities across the supercontinuum spectrum. The spectral performance of the supercontinuum source needs to be improved in support of all future broadband contrast demonstrations.

3. Demonstrations in spectral bands other than 720–880 nm were not possible due to the color and limited spectral range of the supercontinuum source, and due to gold coatings on most of the mirrors (except the newly recoated DM) that could not be replaced without disrupting the flow of TDEM experiments on the HCIT Lyot table. In the future, we recommend that the HCIT migrate to bare aluminum mirror coatings, as the opportunities arise, to support experiments at shorter wavelengths (e.g., with new focal plane masks such as those in Figures 13-15).

4. The scope of our experiments was severely restricted by the relatively short duration of our two 12-week runs. Our October-December 2010 and May-July 2011 experiments were carried out on an intensive day/night and weekends schedule, but we nevertheless completed our runs with many unanswered questions and an unfinished experiment list. We recommend that contiguous periods longer than 12 weeks be the default for future experiment schedules.

5. The dimensions and shapes of the target dark fields should be closely related to science goals. In particular, the "inner box" defined as a 1×1 λ_o/D square area eight years ago for TPF-C milestone #1 is no longer adequate. Current methods of nulling can successfully focus narrowly on improving contrast in just that small box, while generating a suboptimal inner working area. Instead, we will define dark field areas in terms of their outer radial distance from the suppressed central star. We plan to do this in any future TDEM milestone definitions.

6. With a new corrected mask in hand, we are prepared for a new attempt at the milestone demonstration, should the opportunity arise in the HCIT schedule in the future, subject to the following three considerations. (1) The HCIT setup at the outset of a new experiment is critical. If the Lyot table is installed in the chamber, configured for a simple Lyot demonstration, with optical alignments and control hardware and software verified, then a demonstration can be started with minimal (say 2-3 weeks) lead time to establish the nulling and automated calibration procedures. (2) Workforce requirements are minimal. As for previous demonstrations, we would operate with 2 full time (day/night and weekends) experimenters (normally Trauger and Moody), with occasional inputs from the HCIT staff for correction of unforeseen hardware or software infrastructure problems. We would begin with checks of all operating modes in the vacuum. Based on our May-July 2011 run, coming up to speed while dealing with final

details requires 4-6 weeks. As stated in Item 4 above, an overall run time of 12 weeks is a minimum for a successful run if all goes well.

10. References

Balasubramanian, K., "Materials for band-limited image plane masks", Appl. Opt. **47**, 116, 2008.

Give'on, A., B. Kern, S. Shaklan, D. Moody, and L. Pueyo, "Broadband wavefront correction algorithm for high-contrast imaging systems," *Proc. SPIE* **6691**, 66910A, 2007.

Kern, B. *et al.*, "TPF-C Milestone #2 Report," JPL Document D-60951, August 2008.

Kuchner, M., and W. Traub, "A coronagraph with a band-limited mask for finding terrestrial planets," *Astrophys. J.* **570**, 900, 2002.

Moody, D., B.L. Gordon, and J. Trauger, "Design and demonstration of hybrid Lyot coronagraph masks for improved spectral bandwidth and throughput," *Proc. SPIE* **7010**, 70103P, 2008.

Trauger, J. *et al.*, "TPF-C Milestone #1 Report," JPL Document D-35484, July 2006.

Trauger, J. and W. Traub, "A laboratory demonstration of the capability to image an Earth-like extrasolar planet," *Nature* **446**, 771, 2007.

Trauger, J., A. Give'on, B. Gordon. B. Kern, A. Kuhnert, D. Moody, A. Niessner, F. Shi, D. Wilson, and C. Burrows, "Laboratory demonstrations of high-contrast imaging for space coronagraphy," *Proc. SPIE* **6693**, 66930X, 2007.

Trauger, J. *et al.*, "ACCESS – A NASA mission concept study of an Actively Corrected Coronagraph for Exoplanet System Studies," *Proc. SPIE* **7010**, 701029, 2008.

Trauger, J. *et al.*, "ACCESS – A space coronagraph concept for direct imaging and spectroscopy of exoplanetary systems," Public version of the Final Report to the NASA Astrophysics Strategic Concept Studies Program, April 2009.

Trauger, J. *et al.*, "ACCESS – A Concept Study for the Direct Imaging and Spectroscopy of Exoplanetary Systems," in *Pathways towards Habitable Planets, ASP Conf. Series* **430**, 375, 2010; and *Proc. SPIE* **7731,** 773128, 2010.

Trauger, J. *et al.*, "A hybrid Lyot coronagraph for the direct imaging and spectroscopy of exoplanet systems: recent results and prospects." *Proc. SPIE* **8151**, 81510G, 2011.

Trauger, J. *et al.*, "Complex apodization Lyot coronagraphy for the direct imaging of exoplanet systems: design, fabrication, and laboratory demonstration." *Proc. SPIE* **8442**, 84424Q, 2012.

11. Acronyms

ACCESS = Actively-corrected Coronagraph Concept for Exoplanet System Studies

BW = spectral Bandwidth

CCD = Charge Coupled Device

DM = Deformable Mirror

EFC = Electric Field Conjugation

HCIT = High Contrast Imaging Testbed

IWA = Inner Working Angle

OAP = Off Axis Paraboloidal mirror

OD = Optical Density

OWA = Outer Working Angle

PROPER = IDL-based optical propagation code

TDEM = Technology Development for Exoplanetary Missions

TPF-C = Terrestrial Planet Finder Coronagraph